Eur. Phys. J. Plus (2022) 137:1345
https://doi.org/10.1140/epjp/s13360-022-03554-1

THE EUROPEAN PHYSICAL JOURNAL PLUS

Regular Article

Structural, elastic, mechanical, and thermodynamic characteristic of $NaReO_3$ and $KReO_3$ perovskite oxides from first principles study

D. Behera[1], A. Dixit[2], K. Kumari[3], A. Srivastava[4], R. Sharma[5,a], S. K. Mukherjee[1], R. Khenata[6], A. Boumaza[7], S. Bin-Omran[8]

[1] Department of Physics, Birla Institute of Technology, Mesra, Ranchi, Jharkhand, India
[2] Department of Basic Science and Humanities, Pranveer Singh Institute of Technology, Kanpur, Uttarpradesh, India
[3] Department of Electronics and Communication, G.C.R.G Engineering group of Institutions, Lucknow, Uttarpradesh, India
[4] Department of Mechanical Engineering, Shambhunath Institute of Engineering and Technology, Prayagraj, Uttarpradesh, India
[5] Department of Applied Science, Feroze Gandhi Institute of Engineering and Technology, Raebareli, Uttarpradesh, India
[6] Laboratoire de Physique Quantique de la Matière et de la Modélisation Mathématique (LPQ3M), Université de Mascara, 29000 Mascara, Algeria
[7] Laboratoire LPR, Département de Physique, Faculté des Sciences, Université Badji Mokhtar, Annaba, Algeria
[8] Department of Physics and Astronomy, College of Science, King Saud University, P.O. Box 2455, Riyadh 11451, Saudi Arabia

Received: 22 September 2022 / Accepted: 30 November 2022

Abstract The density functional theory was used in the present study to analyse the structural, electronic, mechanical and thermodynamic properties of the perovskite oxides $XReO_3$ (where X = Na and K). This was done in order to learn more about perovskite oxides. The generalized gradient approximation GGA parametrized by Perdew, Burke, and Ernzerhof has been applied in order to carry out structural optimization. It was observed that both of these compounds have a cubic structure. The results of the GGA calculations on the electronic properties of the materials showed that both compounds have a metallic nature. The computed mechanical properties of the perovskite oxides $XReO_3$ (where X = Na and K) demonstrate its stability. The ductile nature of $NaReO_3$ and the brittle nature of $KReO_3$ are shown by the Poisson's ratio (v), the Cauchy's pressure (C_{12}–C_{44}), and the Pugh ratio (B/G), respectively. It was revealed that $NaReO_3$ and $KReO_3$ are anisotropic and isotropic in terms of the elastic properties, respectively. The thermodynamic properties, such as the specific heat capacity, thermal expansion, the Grüneisen parameter, and the Debye temperature, have also been studied in the temperature range of 0–1200 K and the pressure range of 0–161 GPa. According to the findings of the computations, the melting temperatures of $XReO_3$ (where X = Na and K) are, respectively, 285 and 281.4 K. All of these different kinds of data were utilized in the process of analysing the substance. There has been no research done on the proposed compounds as of yet.

1 Introduction

Perovskites are a family of materials that may be differentiated from other types of materials due to the crystal structures of their perovskite crystals, which are analogous to $CaTiO_3$ crystal structures. It was first found in Russia in 1839 by Gustave Rose, and the name "perovskite" was given to the mineral in honour of a Russian mineralogist who went by the name L.A. Perovski [1]. The class of naturally occurring compounds known as perovskites can be identified by their overarching chemical formula, which is written as ABX_3, and they are given the name perovskite. Perovskite oxides, on the other hand, have structures that are denoted by the generic formula ABO_3 [2–5]. The formation of perovskite occurred spontaneously and took the form of halides and oxides, both of which can be found in significant amounts. In the realm of technology, the most cutting-edge ones have a big impact and can be applied in a variety of contexts. The structural and compositional diversity of these materials greatly influences their characteristics [6–8]. Both experimentalists and theoreticians are currently looking for perovskite compounds that can improve their performance for specific functionalities and suit the needs of specific applications [9–11]. This is of paramount importance to the field of materials science; halide perovskites, for instance, are being put to use in solar cell applications [4–7]. Transducers, solar cells, ferroelectric, and piezoelectric devices all benefit greatly from the use of oxide-based perovskites because of the material's versatility. There is a wide variety of perovskites, all of which share the general formula ABO_3 (where the A atom is 9–12-fold coordinated by oxygen, the B atom is sixfold coordinated by oxygen, and BO_6 octahedra are corner-connected. The majority of these devices are made from lead-based materials like $PbTiO_3$, $Pb(Zr,Ti)O_3$, and $Pb(Mg,Nb)O_3$. The fact that lead is poisonous restricts the ways in which it can be used in modern gadgets. It is necessary to develop alternatives to lead-based materials that have the same structure as well as other physical qualities [12, 13]. There has been a lot of research done on lead-free perovskites because of their high strain capacities

[a] e-mail: sharmadft@gmail.com (corresponding author)

Published online: 15 December 2022

and wide range of practical applications [14–17]. Examples of these uses can be found in aeroplanes, nanoelectronics devices, waveguides, actuators, and sensors. Furthermore, these materials have received a lot of attention due to the ease with which they can be synthesized, the unique electrical structure findings that they provide, and their physical properties. These desirable qualities can be attributed, in large part, to the highly correlated electrons in the d and f bands as well as the strong electron-lattice couplings [18]. These materials have found significant use in a wide range of devices and industries, including optoelectronics, thermoelectric, and laser frequency doubling waveguide, making them ideal for cutting-edge technological applications [19–21]. Other examples of applications include laser frequency doubling waveguides. High-temperature superconductors, colossal magneto-resistors, and multiferroic materials are only some of the out-of-the-ordinary uses proposed for these materials [22–25]. The aforementioned studies highlight the advancement in the precision of first-principles calculations on ABO_3 perovskite compounds. Although these compounds initially seem to have many degrees of freedom and complexity, first-principle calculations have made it simpler to comprehend the structure and several distinctive properties of these compounds. Possibilities for the creation of innovative materials are opened up by understanding at the microscopic level. First-principles calculations can provide a more accurate link between the real system and the simplified model to comprehend the underlying physics, resulting in conceptual advancements and greater interaction between theory and experiment. In the current study, we examined two distinct ABO_3-based perovskite compounds that include $XReO_3$ (where X = Na and K). This study presents a comparative analysis of the aforementioned content. Utilizing Density Functional Theory, we examined its elastic, mechanical, and thermodynamic properties for industrial purposes (DFT). In addition, properties are investigated under FP-LAPW-GGA (PBE). The recommended materials were examined for the first time. First investigations have been carried out into the cubic compounds $NaReO_3$ and $KReO_3$. There is currently no data available for the suggested materials.

2 Computational method

The density functional theory (DFT) has been shown to be the most influential, acceptable, and approximate method for describing the physical properties of solids [26, 27]. The Full-potential Linearized Augmented Plane Wave (FPLAPW) method [28], which is built into WIEN2k [29], is used to determine the physical properties of the present perovskite oxide $XReO_3$ (where X = Na and K). Within the framework of the Perdew, Burke, and Ernzerhof (PBE) method [30], the generalized gradient algorithm (GGA) was used to optimize the structures of the perovskite compounds $XReO_3$ (where X = Na and K). The structural properties of $XReO_3$ perovskites were examined and measured at a mesh size of 1000 k-points ($10 \times 10 \times 10$). The value of $K_{max} \times R_{MT}$ can be predicted with the help of the convergence test. This test assumes that the calculation has converged if ($K_{max} \times R_{MT} = 7.0$), where R_{MT} is the diameter of the muffin tin and K_{max} is the cut-off for plane waves in the reciprocal lattice vector. The following expressions that represent the radius of a muffin tin for each atom were chosen to be: $R_{MT} = 2.22$, Na = 2.01, Re = 1.98, and O = 2.06 The Charpin method [31] was employed for the elastic constants. The calculation was done at the equilibrium lattice constants, which are found by plotting the total energy against the unit cell volume and fitting that to the Birch–Murnaghan equation of state [32]. To compute the elastic properties of the studied $XReO_3$ (where X = Na and K) compounds IRELAST method as implemented in WIEN2K code [33, 34]. The quasi-harmonic Debye model [35] is presented here in order to determine the thermodynamic characteristics of the cubic compound $XReO_3$ (where X = Na and K).

3 Results and discussion

3.1 Structural properties

In this set of computations, the ground-state stable structure at 0 GPa pressure is taken into consideration. This structure has the atomic positions (X = Na and K) at (0, 0, 0); O at (1/2, 1/2, 0); (1/2, 0, 1/2); and (0, 1/2, 1/2); and Re at (1/2, 1/2, 1/2) in its cubic Pm-3m structure as shown in Fig. 1. The energy-volume optimization was accomplished by using the Birch–Murnaghan equation to determine the lattice parameters, which were then used to calculate the thermodynamic properties of the present oxides $NaReO_3$ and $KReO_3$ within the quasi-harmonic Debye model [36]. This allowed for the achievement of the energy-volume optimization goal. In order to determine the ground state parameters of $NaReO_3$ and $KReO_3$, we fit the data to Murnaghan's equation of state [32], which is depicted in Fig. 2 as the total energy as a function of the volume of the unit cell. These ground state properties include the equilibrium lattice parameter (a_0), total energies (E_0), bulk modulus (B_0), and its pressure derivatives (B_0'). Table 1 provides a summary of the previously acquired results as well as the computed parameters of the ground state that were obtained by applying the GGA approach. When we compare our findings to those of earlier theoretical calculations, we find that there is a high degree of congruence between the two sets of data. This was discovered when we performed an analysis of the results of B_0 and B'. As a result of our work, we have determined that the optimized lattice parameters for $NaReO_3$ are $a = 3.887$ Å, whereas the optimized lattice parameters for $KReO_3$ are $a = 3.930$ Å, respectively. It is important to keep in mind that when the atomic number increases from K to Na, the lattice parameters also increase. The accumulation of electron layers is to blame for this phenomenon. It is thought that the equilibrium volume of $XReO_3$ (X = Na, K) cubic perovskite will be controlled by a certain type of XRe sub-lattice. Figure 2

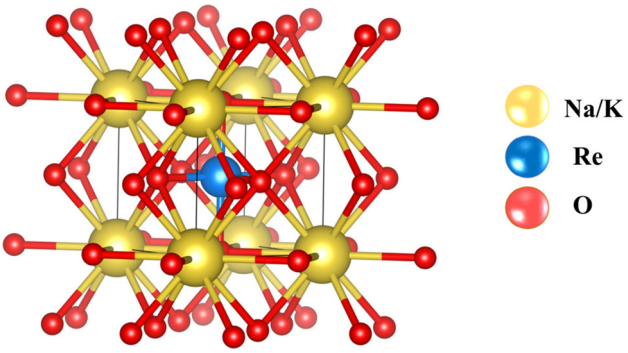

Fig. 1 Crystal structure of $XReO_3$(X = Na, K)

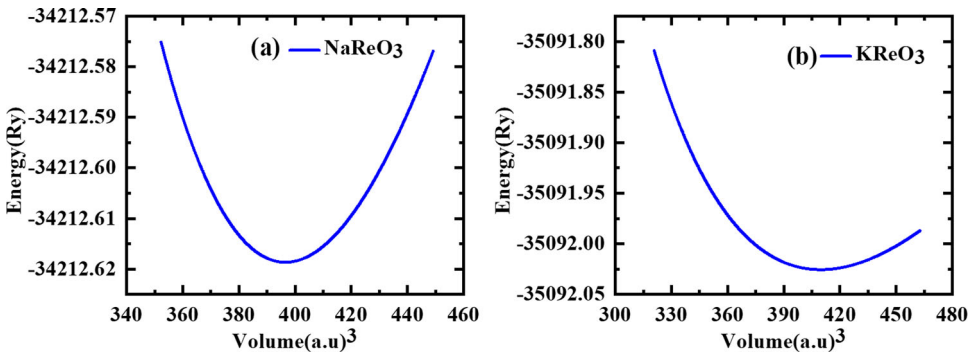

Fig. 2 Energy versus volume in PBE-GGA: **a** $NaReO_3$, **b** $KReO_3$

Table 1 Ground state structural parameters of the $XReO_3$ (X = Na, K) by PBE-GGA

Parameters	$NaReO_3$	$KReO_3$	$RbReO_3$ [37]
Lattice constant (Å)	3.8877	3.9300	3.989
Volume (Å^3)	396.5259	409.6054	428.49
Pressure B (GPa)	214.5457	206.4147	200.62
Pressure derivative B'	3.7804	4.7233	6.61
Minimum total energy per unit cell (Ry)	− 34,212.618656	− 35,092.025522	− 39,850.6
Bond length (Å)	Na–O = 2.74 Re–O = 1.94 Na–Re = 3.36	K–O = 2.78 Re–O = 3.41 K–Re = 1.96	
Formation energy (eV/atom)	− 1.939	1.975	
Cohesive energy (eV/atom)	4.84	4.86	

demonstrates that the ground state of $KReO_3$ is the most energy-efficient compared to $NaReO_3$. In $NaReO_3$ant perovskites, the inter-atomic distances are Na–O = 2.74 Å, Re–O = 1.94 Å and Na–Re = 3.36 Å, whereas in $KReO_3$, the inter-atomic distances are K–O = 2.78 Å, Re–O = 1.96 Å and K–Re = 3.41 Å. This indicates that the directional O–Re bonds in ($NaReO_3$ or $KReO_3$) ought to be the strongest. The formation energy (E_f) is written as the difference between the total energy (E_T) and the sum of the atomic energies of all the individual atoms at the stable crystal structure as follows:

$$E_{\text{form}}^{\text{XReO}_3} = E_T - \left[E_{X=\text{Na, K}} + E_{\text{Re}} + 3E_O\right] \quad (1)$$

The computed values of formation energies are − 1.932 eV/atom, − 1.920 eV/atom, which is conducive to the crystal favourable allowing stability for the cubic oxide perovskite $XReO_3$ (X = Na, K).

3.2 Electronic properties

Electronic results (band structure and density of state results) for all of these materials have been calculated in PBE-GGA. The bandgap in the band structure may have a role in the explanation for the electron transition [38–40]. Band structures are depicted in the region of maximum symmetry defined by the Brillouin zone. Figure 3a, b shows the band structure results for $XReO_3$ (X = Na, K). Results from the study of the band structure show that both compounds are metallic with no energy separation between the conduction and valence bands. Both compounds were discovered to have electrons at the Fermi level. The density of states (DOS) provides illustrative evidence of the band structure conclusions reached for these substances [41, 42]. DOS diagrams (Fig. 3a, b)

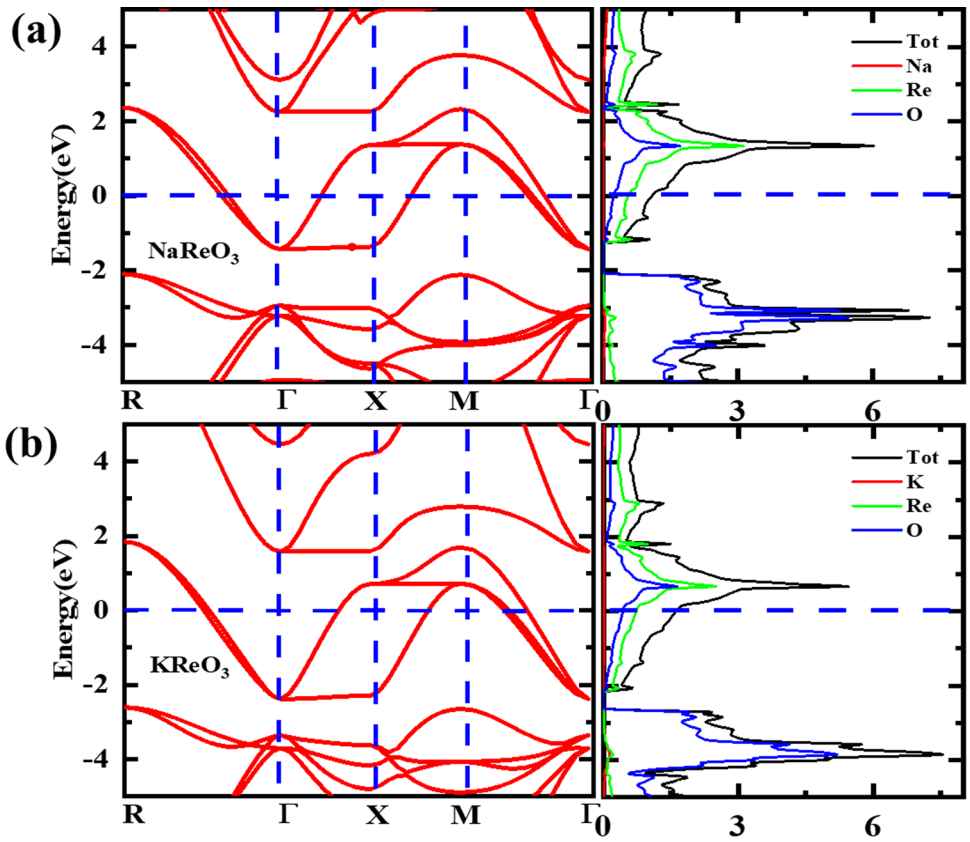

Fig. 3 Band structure, Total and partial density of states within PBE-GGA: **a** $NaReO_3$ and **b** $KReO_3$

have been produced for $XReO_3$ (X = Na, K) to help make the band results more evident. DOS data for Na–p, K–p, Re–p, d, and O–p have been plotted. DOS readings reveal nearly identical metallic characteristics for both compounds. It was observed that both the Re–d and O–p states pass the Fermi level in each of these compounds, which explains why they have a metallic quality. Bands generated by Na and K atoms at X sites are located in the valence or conduction band, respectively. The Na-p states of $NaReO_3$ can be seen in the 1–4 eV conduction band region of Fig. 3a. Figure 3b shows that the Cs–d states of KReO3 are in the 0–4 eV region of the conduction band. Figure 3a, b shows the nature of compound is metallic.

3.3 Elastic and mechanical properties

The mechanical stability, hardness, plastic twist, and other aspects of a material's mechanical properties can all be greatly impacted by the material's elastic constants, which are always considered to be fundamental for the purpose of understanding the essential features that comprise its mechanical properties. The elasticity values for $XReO_3$ (where X = Na and K) perovskite compounds have been computed using the Charpin technique [31], which has been implemented in the WIEN2k package [29]. These calculations have been done under ambient pressure. Elastic constants have been computed with the assistance of the GGA. Because both compounds are stable in the cubic phase, the mechanical stability has been proven by lowering the number of dependent elastic constants from 21 to just three independent elastic constants. These three independent elastic constants are represented by the symbols C_{11}, C_{12}, and C_{44}. The stability requirements for the cubic phase are as follows, and it was discovered that the computed values of these elastic constants [43, 44] match those requirements.

$$(C_{11}-C_{12}) > 0, \tag{2}$$

$$C_{11} > 0, \tag{3}$$

$$C_{44} > 0, \tag{4}$$

$$(C_{11} + 2C_{12}) > 0, \tag{5}$$

$$C_{12} < B < C_{11} \tag{6}$$

The computed values of elastic constants are shown in Table 2, and it is evident that the mentioned restrictions of the elastic value are properly followed by both of the compounds; as a result, they are mechanically stable [45]. This is because both compounds

Table 2 Values of elastic constants (C_{ij}), bulk modulus (B), shear modulus (G), Young's modulus (Y), Poisson's ratio (σ), Pugh ratio, Frantsevich ratio, Shear anisotropy factor (A) Cauchy pressure C^P, sound velocities (m/s), Debye Temperature Θ_D (K) of $XReO_3$(X = Na, K)

Material property	$NaReO_3$	$KReO_3$	$RbReO_3$ [37]
C_{11} (GPa)	476.04	301.37	388.93
C_{12}(GPa)	87.05	76.12	117.92
C_{44}(GPa)	77.74	112.81	91.91
Bulk modulus, B (GPa)	216.17	151.206	208.3
Shear modulus, G (GPa)	113.80	112.74	107.41
Young modulus, Y (GPa)	289.63	270.89	274.98
Poisson ratio, σ (GPa)	0.277	0.201	0.27
Pugh ratio, B/G (GPa)	1.89	1.34	1.939
Frantsevich ratio, G/B (GPa)	0.52	0.74	
Shear anisotropy factor, A (GPa)	0.399	1.00	0.67
Cauchy pressure C^P(GPa)	9.31	− 36.69	
Transverse sound velocity (m/s)	3951.04	3883.79	
Longitudinal sound velocity(m/s)	7117.11	6351.54	
Average sound velocity (m/s)	4400.74	4288.28	
Temperature Θ_D (K)	576.13	555.44	
Melting temperature T_m(K)	3366.42	2334.13	2851

adhere to the mentioned restrictions of the elastic value. There are many mechanical properties that may be calculated with the use of the elastic constants and their values. The Young's modulus (Y), the shear modulus (G), the bulk modulus (B), and the Poisson's ratio are all examples of such characteristics (v). In order to examine the material's stiffness, plastic twist, and strength, certain conditions must be met. Utilizing the computed values of elastic constants is required in order to derive Hill's shear modulus G_H; this modulus is an arithmetic mean of the (G_R) Reuss and (G_V) Voigt approximations [46].

These mechanical characteristics and their derived values are listed in Table 2. It is necessary to measure the Young's modulus (Y) and bulk modulus (B) of the material in order to get its hardness and strength. Calculated values for $XReO_3$ (X = Na and K) are 289.63 and 270.89 GPa, respectively. We have also determined the bulk modulus for these substances. In the case of XReO3 (X = Na and K), the computed values of B are 216.17 and 151.206 GPa, respectively. Young's modulus and bulk modulus measurements show that both compounds are sufficiently stiff and robust. Therefore, these compounds can be used to create electrode materials for fuel cells and may play an essential role in the production of ultra-hard devices. The ductility of these materials was determined by calculating the ratio of their bulk modulus to their shear modulus (B/G), which was a concept put forth by Pugh [47]. Pugh's criteria state that a material is considered to have ductile behaviour if the B/G ratio of the material is more than 1.75; otherwise, the material is considered to have brittle behaviour [47]. The computed value of B/G for $XReO_3$ (where X = Na and K) came out to be 1.89, and the respective value for G was found to be 1.34. As a result of this, it is evident from the B/G value that $NaReO_3$ will have a ductile nature, but $KReO_3$ would behave in a brittle manner. Cauchy's pressure (C_{12}–C_{44}) value has been examined further in order to gain a better understanding of the ductility and brittleness of this material. If the value of this parameter is positive, it indicates that the material is ductile; otherwise, it indicates that the material is brittle [48]. The value that was computed for (C_{12}–C_{44}) turned out to be positive for $NaReO_3$, while the value that was calculated for $KReO_3$ turned out to be negative. Therefore, it was determined, based on Pugh's criteria as well as Cauchy's pressure that $NaReO_3$ will exhibit a ductile character, whereas $KReO_3$ will demonstrate a brittle nature. Poisson's ratio is an additional characteristic that helps to designate the ductility and brittleness of a material. The Frantsevich rule states that brittle behaviour is exhibited by a material if it is less than 0.26 and the substance is not otherwise ductile. It was determined that the value of for $NaReO_3$ was greater than or equal to 0.26, but the value for $KReO_3$ was less than or equal to 0.26. Therefore, according to, $NaReO_3$ should be considered ductile, whereas $KReO_3$ should be considered brittle, as seen in Table 2. Also, Poisson's ratio can be used to learn about the bonding structure of a substance. If the value of this ratio is less than 0.10, the bonding in the material is said to be covalent; if it is between 0.25 and 0.33, the bonding is said to be ionic; and if it is larger than 0.33, the material is said to be metallic. The value of drops to 0.277 as a consequence of our experiments, which is extremely near to 0.25 for $NaReO_3$ and 0.201 for $KReO_3$; thus, $NaReO_3$ and $KReO_3$ will exhibit ionic bonding. We have determined the anisotropic factor A, stands for the elastic anisotropy and isotropy. This is part of our ongoing effort to gain a better understanding of the characteristics of elasticity in various directions. If a material is isotropic, then its value of A will be equal to unity; if it is anisotropic, then it will have a value that deviates from unity. For the $NaReO_3$ compound, the calculated value of A is non-unity, but for the $KReO_3$ compound, it is 1. In this way, $NaReO_3$ will exhibit elastic anisotropy, whereas $KReO_3$ maintains elastic isotropy. We have also determined the melting point (T_m) for these substances. In terms of its physical qualities, as shown by Cauchy's pressure C_P, it has been demonstrated that $KReO_3$ is more brittle than $NaReO_3$. Another illustrative way to demonstrate the elastic anisotropy of any material is by visualizing the mechanical moduli in three-dimensional (3D) surface. For a cubic crystal,

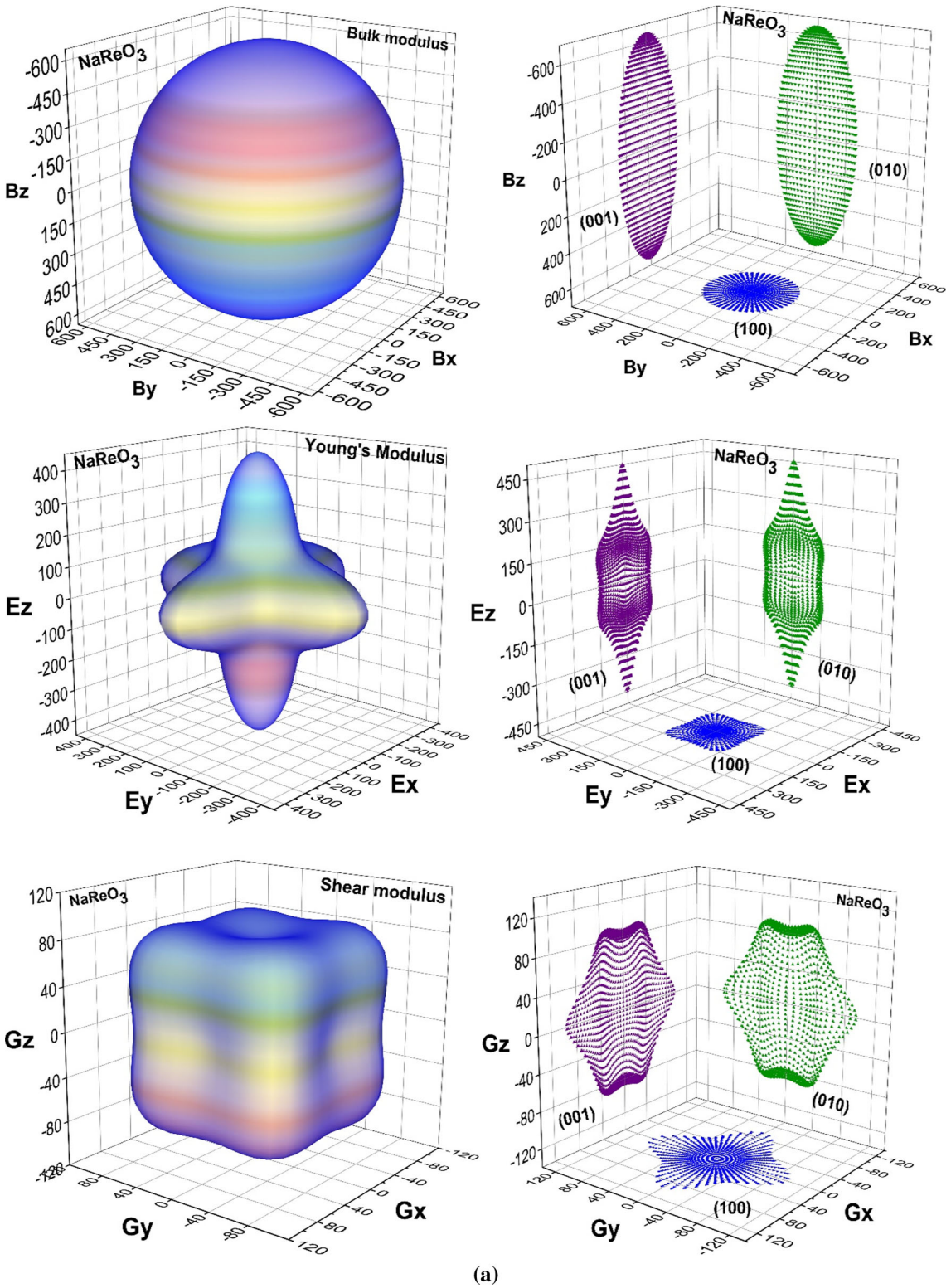

(a)

Fig. 4 **a** 3D-directional representation of the Bulk modulus (*B*, in GPa), Young modulus (*E* in GPa) and Shear modulus (*G*, in GPa) and their projections in different planes (100), (010) and (001) for $NaReO_3$. **b** 3D-directional representation of the Bulk modulus (*B*, in GPa), Young modulus (*E* in GPa) and Shear modulus (*G*, in GPa) and their projections in different planes (100), (010) and (001) for $KReO_3$

the crystallographic direction dependence of the bulk modulus *B*, Young's modulus *E* and shear modulus *G* are computed by using the following expressions:

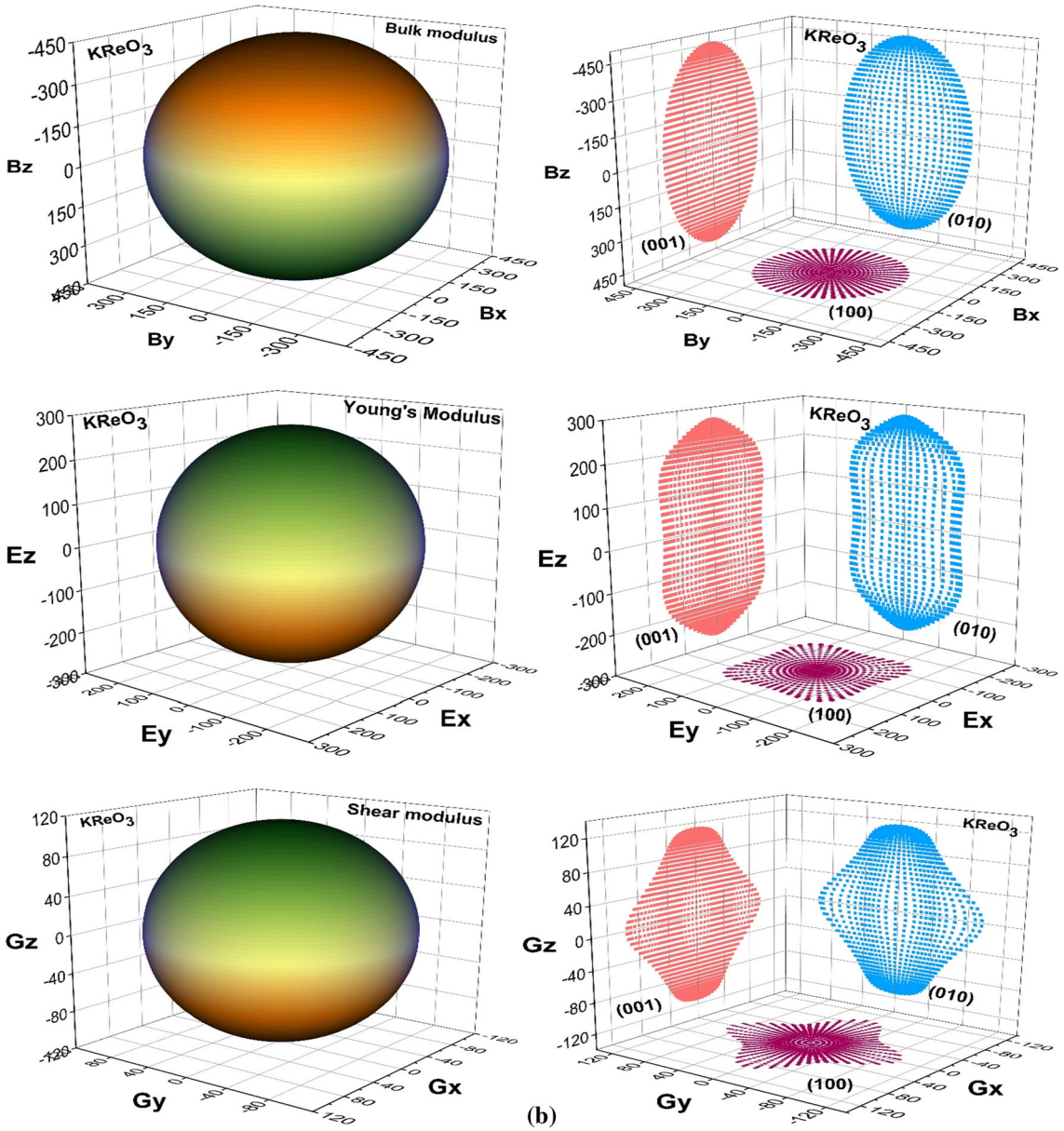

Fig. 4 continued

$$\frac{1}{B} = (S_{11} + 2S_{12})\left(l_1^2 + l_2^2 + l_3^2\right) \tag{7}$$

$$\frac{1}{E} = S_{11} - 2\left(S_{11} - S_{12} - \frac{1}{2}S_{44}\right)\left(l_1^2 l_2^2 + l_2^2 l_3^2 + l_3^2 l_1^2\right) \tag{8}$$

$$\frac{1}{G} = S_{44} - 4\left(S_{11} - S_{12} - \frac{1}{2}S_{44}\right)\left(\sin^2\theta \cdot \cos^2\theta + 0.125\sin^4\right)(1 - \cos 4\varphi) \tag{9}$$

Here, S_{ij} are the contents of the elastic compliance constants matrix, which are obtained from the inverse of the elastic constant matrix ($S_{ij} = C_{ij}^{-1}$), and their values are depicted in Table 2. l_1, l_2 and l_3 are the direction cosines in accordance with the x-, y- and z-axes, respectively. If the 3D directional-dependent surface is exactly of spherical shape, the material is characterized as isotopic, but if the surfaces are non-spherical, indicating their character as anisotropic. The three-dimensional surfaces with their 2D projections of different planes [100], [010] and [001] of the bulk, Young's and shear moduli for the studied compounds are illustrated in Fig. 4a, b, respectively. As shown in Fig. 4a, b, the 3D plot surface of the bulk modulus represents a perfect spherical form for the title compounds, revealing them as isotropic materials. We can note substantial deviation from the shape of the sphere for the

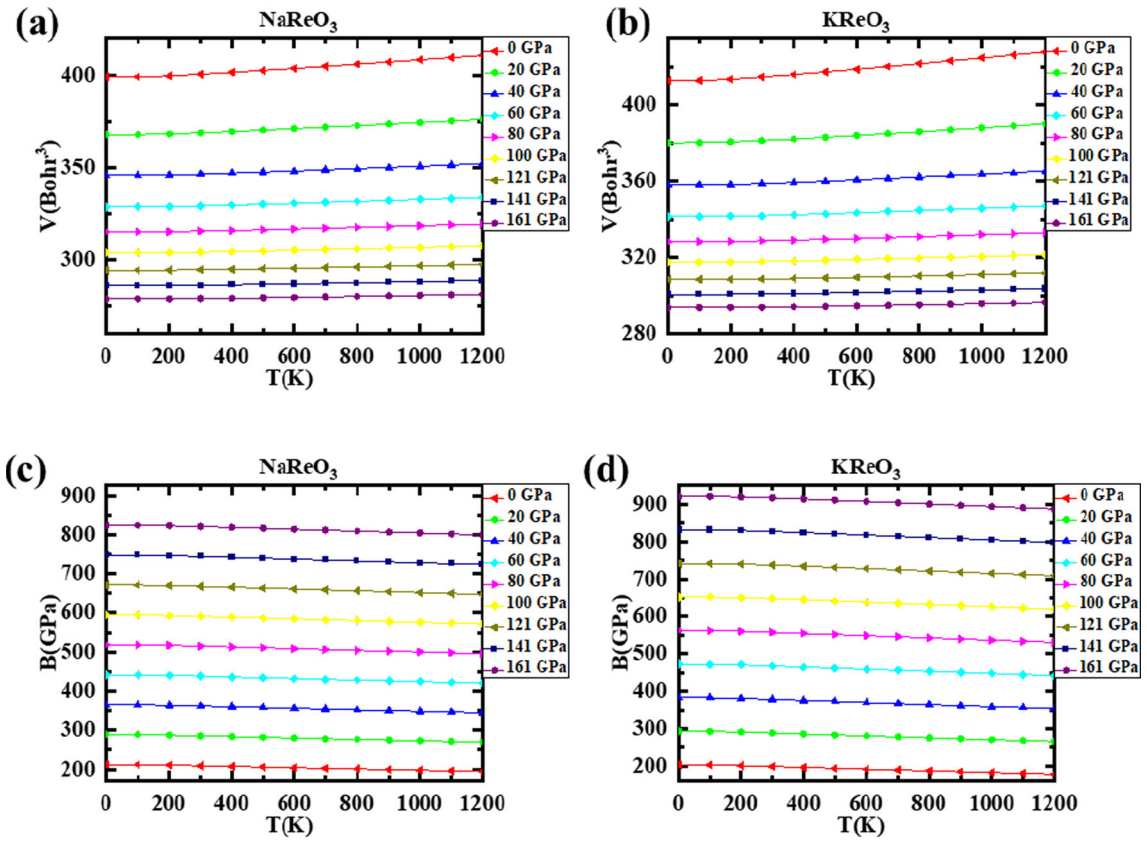

Fig. 5 **a**, **b** Volume (V), **c**, **d** Bulk modulus (B) as a function of temperature and pressure for $XReO_3$ (X = Na, K)

shear modulus and Young's modulus, hence revealing that the shear modulus demonstrates a larger degree of anisotropy. From the 2D plane projections, it is clear that bulk moduli values at different planes have an isotropic character, while the non-circular shape of Young's modulus and shear modulus reveals greater anisotropic behaviour for G than E.

Through the use of elastic constant values, melting temperature (T_m) value has been determined. The melting point values reported in Table 2 show that both the compounds under study have sufficiently high melting points with values 3366.42 for $NaReO_3$ K and 2334.13 K for $KReO_3$ compounds. Table 2 displays the computed values for the melting temperature, the Debye temperature, the average sound velocity, and the transverse sound velocity. According to the results, $NaReO_3$ has a greater Debye temperature than $KReO_3$. As a result, $NaReO_3$ is superior to $KReO_3$ in terms of energy storage capacity. Our calculated values of average sound velocity and are 7117.11 m/s, 3951.04 m/s, 4400.74 m/s and 576.13 K for $NaReO_3$, respectively, while it is 6351.54 m/s, 3883.79 m/s, 4288.28 m/s and 555.44 K for $KReO_3$ within PBE-GGA.

3.4 Thermodynamic properties

The thermodynamic characteristics of $XReO_3$ (X = Na and K) materials are studied here using the quasi-harmonic Debye approximation [49–52] Thermodynamic properties including specific heat at constant volume (C_v), thermal expansion (α), and the Debye temperature (θ_D) have been determined as a function of a pressure range of 0–161 GPa and a temperature range of 0–1200 K (200 K steps) (step size of 20 GPa). It has been shown that the quasi-harmonic Debye model works well for temperatures between 0 and 1200 K. Unit cell volume changes for $XReO_3$ (X = Na and K) as a function of pressure and temperature are shown in Fig. 5a, b. Temperature and pressure have opposite impacts on cell volume for both substances. When the pressure is raised, the volume decreases, but when the temperature rises, the volume expands. It is important to note that, in general, all solids tend to get smaller when they are pressed and bigger when they are heated.

It is commonly known that the stiffness resistance of a material is related to a material's bulk modulus, or B. In Fig. 5c, d, the fluctuation in the value of B has been displayed as a function of both the temperature and the pressure, respectively, for $XReO_3$ (X = Na, K). It can be seen quite linearly from Fig. 5c, d that the value of B remains unaffected by changes in temperature, but it demonstrates an ascending trend in response to reductions in pressure. This holds true for both of the materials that are being taken into account. This increase and decrease in B with pressure and temperature is due to the fact that volume decreases with rising

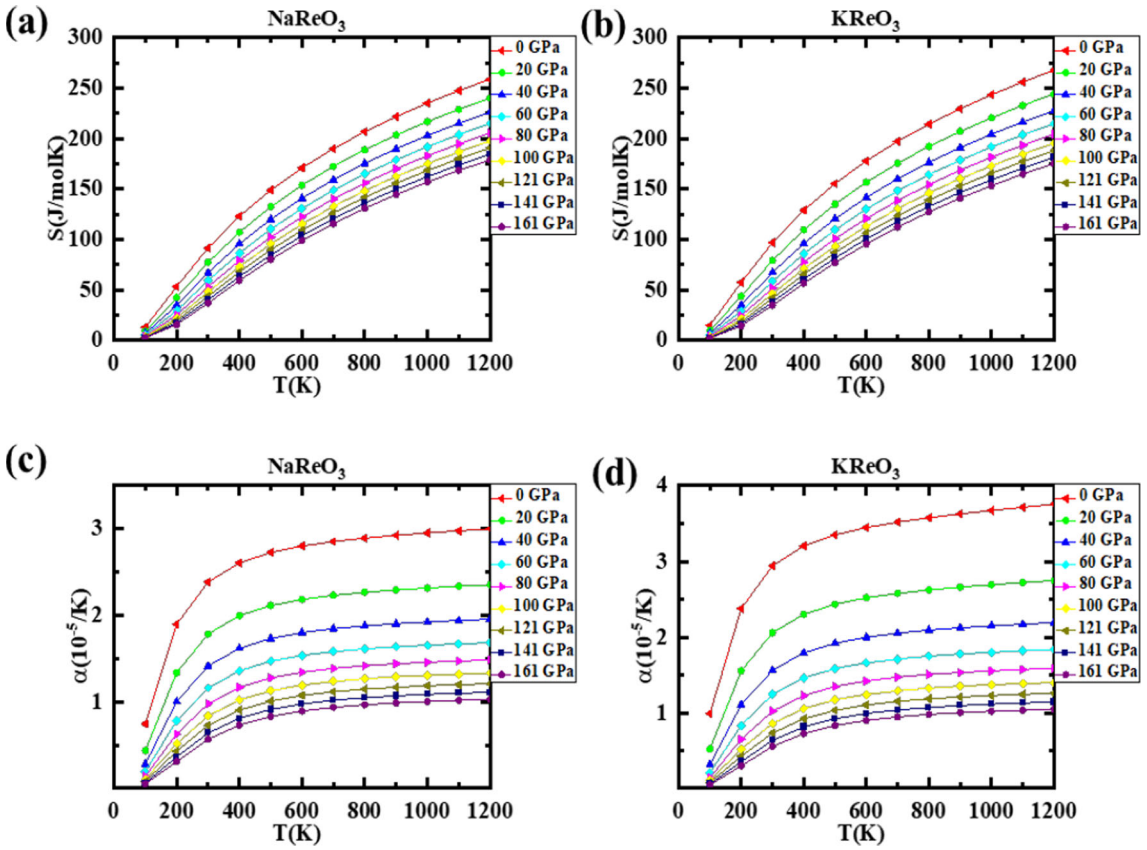

Fig. 6 **a**, **b** Entropy (S), **c**, **d** thermal expansion (α) as a function of temperature and pressure for $XReO_3$ (X = Na, K)

pressure and volume increases with lowering temperature. At 0 GPa of pressure and all temperatures, the calculated value of B for $XReO_3$ (where X = Na and K) was obtained to be 210 and 200 GPa, respectively.

Figure 6a, b depicts the entropy of the proposed materials, which was measured to be 12.0 J/molK at 100 K temperature and maximum at 0 GPa pressure for $NaReO_3$ and 12.5 J/molK at 100 K temperature for the $KReO_3$ compound. Both of these values were found to be maximums. A plot of the thermal expansion coefficient "α" versus temperature and pressure is shown in Fig. 6c, b. These statistics make it very easy to see that the value climbs sharply under low temperatures up to 300 K, whereas it climbs steadily and linearly under high temperatures. This can be seen by comparing the two sets of data. It is possible that this is because of the saturation of up to 300 K. The value for $NaReO_3$ was calculated to be 2.4×10^{-5} per Kelvin, but the value for $KReO_3$ was 3×10^{-5} per Kelvin. It has been discovered that pressure may bring the value down. However, when the temperature is raised, the effect of pressure on the value becomes more prominent and falls more quickly. This is because the quasi-harmonic model does not work well when low pressure and high temperature are both present.

The Gruneisen parameter (γ) was used in order to determine the thermodynamic properties of the material when it was subjected to high temperatures and pressures [53]. This parameter reflects the anharmonicity that exists within the crystal. In addition to this, it depicts the relationship between temperature and pressure in terms of phonon frequencies, also known as vibrational frequencies. As a result, we were finally able to calculate the pressure and temperature dependence of $XReO_3$ (X = Na and K) as shown in Fig. 8a, b. The value of g gradually climbs upward as the temperature continues to rise, while it heads downward as pressure continues to rise. For $NaReO_3$, the value that was estimated under ambient circumstances was found to be 1.73295, and this value remains the same across all temperatures and pressures up to 100 GPa.

There are several additional thermodynamic parameters, such as the solid heat capacity and melting temperature, that are connected to the Debye temperature (θ_D). As shown in Fig. 7c, d, the Debye temperature of $XReO_3$ (X = Na and K) varies with both temperature and pressure. When comparing the two graphs, it is evident that the value of θ_D decreases extremely slowly but nearly becomes constant across a wide range of temperatures and high pressures. At 0 GPa pressure, it is decreasing with rising temperature for both the compounds. The value of θ_D is observed to grow with pressure at a certain temperature. For X = Na and K, the calculated value of θ_D for $XReO_3$ at 0 GPa pressure and 300 K temperature is 575 and 570.05 K, respectively.

The effect of temperature and pressure on the specific heat capacity (C_V) is shown graphically in Fig. 8a, b. One find striking similarities when comparing the C_V diagrams of various substances. At temperatures below 300 Kelvin (K), C_V increases at an exponential rate; from 300 to 700 K, C_V increases at a slower rate; and at temperatures beyond 700 K, C_V is nearly constant.

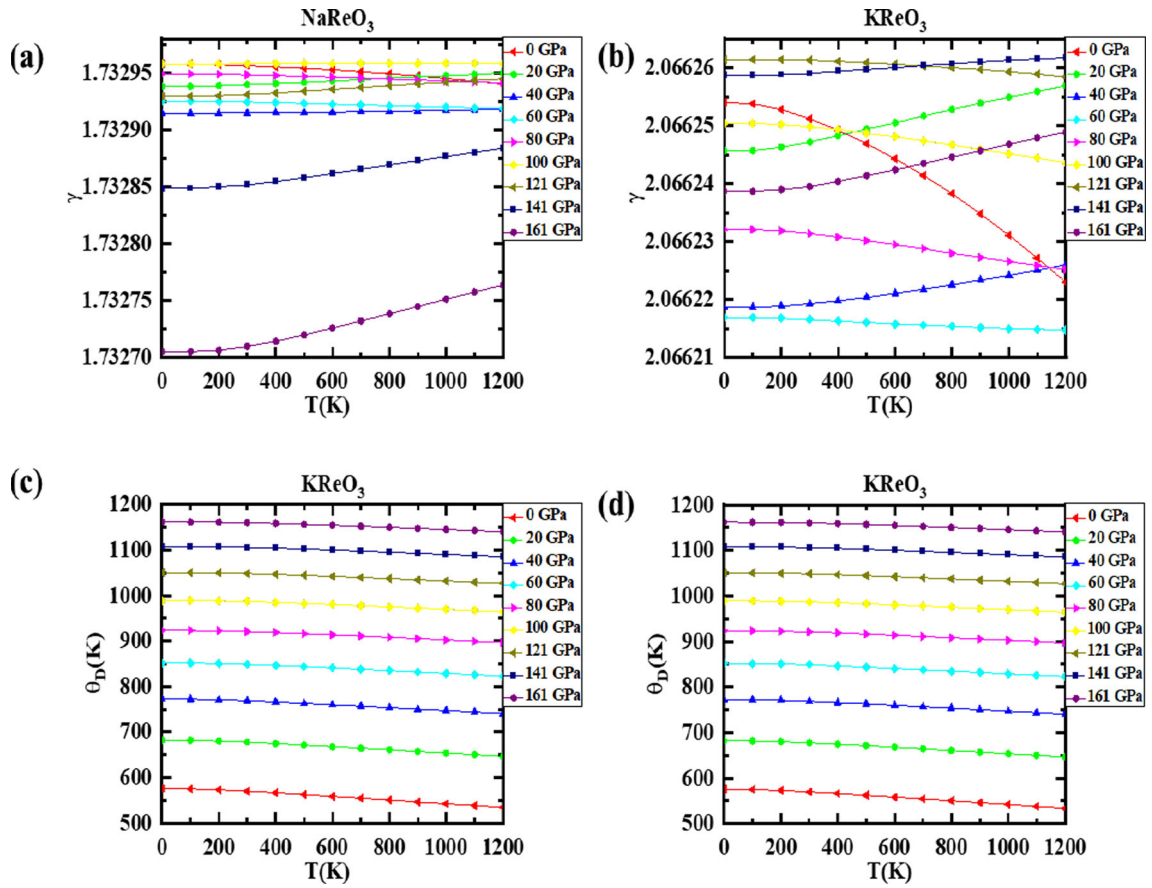

Fig. 7 **a**, **b** Gruneisen parameter (γ) **c**, **d** Debye temperature (θ_D) as a function of temperature and pressure for $XReO_3$ (X = Na, K)

The well-known Debye model ($C_V(T)/T^3$) predicts that C_V will increase at low temperatures. This is because it is only the long-wavelength vibration modes of the lattice that are occupied, and it is possible to approach these modes if the lattice is treated as a continuum [54]. However, the classical conduct ($C_V(T)/3R$ for mono-atomic materials) is found at sufficiently high temperatures, as predicted by Petit and Dulong's law [55]. The computed values of C_V at 0 GPa and 300 K were found to be 104 and 105 (J mol^{-1} K), respectively, for $XReO_3$ (X = Na and K).

The heat capacity C_p temperature diagram is depicted in Fig. 8c, d, which shows the relationship between the two variables at varying pressures. The fluctuation characteristics of C_p values at lower temperatures, which are comparable to those of C_v, become more pronounced as the temperature rises. The change in C_p, on the other hand, behaves differently from the change in C_v when the temperature is high. The critical pressure (C_p) values drop when the pressure is increased and do not converge to a single value. When the temperature is raised, there is a discernible rise in the heat capacity.

4 Conclusions

In this work, we have performed ab initio calculations on the structural, elastic, and thermodynamic properties for the cubic $XReO_3$ (X = Na and K) using the FP-LAPW method. The exchange correlations PBE-GGA has been used to predict the structural ground state details. The structural ground state details have been predicted using the exchange correlation PBE-GGA. The computed lattice constant and bulk modulus, as well as other ground-state parameters, are in good agreement with the other available theoretical results. According to the electrical structure calculations, cubic $XReO_3$ (X = Na and K) has a zero-band gap and show metallic behaviour. Young's modulus and bulk modulus are two measures of the brittleness of the materials in both the compounds, and both can be used in the construction of fuel cell electrodes. The cubic compound $NaReO_3$ is found to be ductile, whereas $KReO_3$ was found brittle from the Poisson's ratio (ν), Cauchy's pressure (C_{12}–C_{44}), and Pugh ratio (B/G). The $NaReO_3$ compound was found to be elastically anisotropic, whereas $KReO_3$ maintains elastic isotropy. Through the quasi-harmonic Debye model, the dependence of the bulk modulus, lattice constant, specific heat capacities and Debye temperature on pressure and temperature have been predicted.

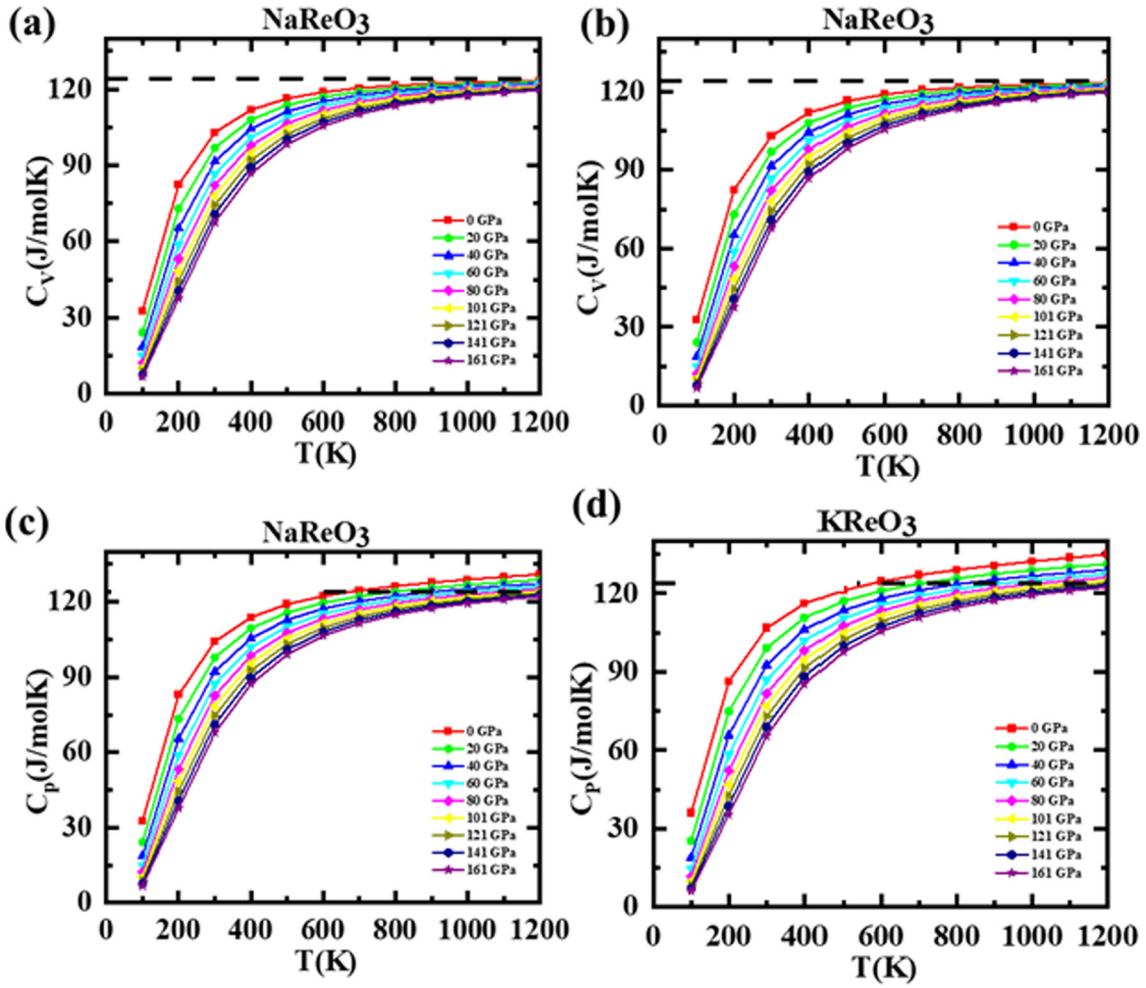

Fig. 8 **a**, **b** Specific heat capacity at constant volume (C_v), **c**, **d** specific heat capacity at constant pressure (C_p) as a function of temperature and pressure for $XReO_3$ (X = Na, K)

Acknowledgements The author Bin Omran acknowledges Researchers Supporting Project number (RSP-2021/82), King Saud University, Riyadh, Saudi Arabia.

Data Availability Statement This manuscript has associated data in a data repository. [Authors' comment: Data will be available on reasonable request through corresponding author.]

References

1. E.A. Katz, Perovskite: name puzzle and German-Russian odyssey of discovery. Helv. Chim. Acta **103**, e2000061 (2020)
2. C. Li, K.C.K. Soh, P. Wu, Formability of ABO_3 perovskites. J. Alloys Compd. **372**, 40–48 (2004)
3. R.S. Roth, Classification of perovskite and other ABO_3-type compounds. J. Res. Natl. Bur. Stand. **58**, 75 (1957)
4. A. Dey, R. Sharma, S.A. Dar, I.H. Wani, Cubic $PbGeO_3$ perovskite oxide: a compound with striking electronic, thermoelectric and optical properties, explored using DFT studies. Comput. Condens. Matter **26**, e00532 (2021)
5. R. Yadav, A. Srivastava, R. Sharma, J.A. Abraham, S.A. Dar, A.K. Mishra, V. Srivastava, The study of optical and thermoelectric behaviour of thalium based flouropervoskite ($TlSiF_3$) for photovoltaic and renewable energy applications by DFT. J. Solid State Chem. **313**, 123266 (2022)
6. M.A. Pena, J.L.G. Fierro, Chemical structures and performance of perovskite oxides. Chem. Rev. **101**, 1981–2018 (2001)
7. M.A. Green, A. Ho-Baillie, H.J. Snaith, The emergence of perovskite solar cells. Nat. Photonics **8**, 506–514 (2014)
8. R. Sharma, A. Dey, S.A. Dar, V. Srivastava, A DFT investigation of $CsMgX_3$ (X = Cl, Br) halide perovskites: electronic, thermoelectric and optical properties. Comput. Theor. Chem. **1204**, 113415 (2021)
9. A. Kojima, K. Teshima, Y. Shirai, T. Miyasaka, Organometal halide perovskites as visible-light sensitizers for photovoltaic cells. J. Am. Chem. Soc. **131**, 6050–6051 (2009)
10. H.-S. Kim, C.-R. Lee, J.-H. Im, K.-B. Lee, T. Moehl, A. Marchioro, S.-J. Moon, R. Humphry-Baker, J.-H. Yum, J.E. Moser, Lead iodide perovskite sensitized all-solid-state submicron thin film mesoscopic solar cell with efficiency exceeding 9%. Sci. Rep. **2**, 1–7 (2012)
11. J. Burschka, N. Pellet, S.-J. Moon, R. Humphry-Baker, P. Gao, M.K. Nazeeruddin, M. Grätzel, Sequential deposition as a route to high-performance perovskite-sensitized solar cells. Nature **499**, 316–319 (2013)

12. A.A. Emery, C. Wolverton, High-throughput DFT calculations of formation energy, stability and oxygen vacancy formation energy of ABO_3 perovskites. Sci. Data **4**, 1–10 (2017)
13. S.B. Patel, A. Srivastava, R. Sharma, J.A. Abraham, V. Srivastava, Prediction of structural, electronic, mechanical, thermal, and thermoelectric properties in $PbMO_3$ (M = Sb, Bi) perovskite compounds: a DFT study. Eur. Phys. J. Plus **137**, 380 (2022)
14. A.A. Mubarak, S. Al-Omari, First-principles calculations of two cubic fluoropervskite compounds: $RbFeF_3$ and $RbNiF_3$. J. Magn. Magn. Mater. **382**, 211–218 (2015)
15. P. Ravindran, R. Vidya, A. Kjekshus, H. Fjellvåg, O. Eriksson, Theoretical investigation of magnetoelectric behavior in $BiFeO_3$. Phys. Rev. B **74**, 224412 (2006)
16. H. Zhang, W. Jo, K. Wang, K.G. Webber, Compositional dependence of dielectric and ferroelectric properties in $BiFeO_3$–$BaTiO_3$ solid solutions. Ceram. Int. **40**, 4759–4765 (2014)
17. W. Eerenstein, N.D. Mathur, J.F. Scott, Multiferroic and magnetoelectric materials. Nature **442**, 759–765 (2006)
18. A. Abbad, W. Benstaali, H.A. Bentounes, S. Bentata, Y. Benmalem, Search for half-metallic ferromagnetism in orthorhombic $Ce(Fe/Cr)O_3$ perovskites. Solid State Commun. **228**, 36–42 (2016)
19. M.E. Lines, A.M. Glass, *Principles and Applications of Ferroelectrics and Related Materials* (Oxford University Press, Oxford, 2001)
20. C. Moure, O. Peña, Recent advances in perovskites: processing and properties. Prog. Solid State Chem. **43**, 123–148 (2015)
21. G. Murtaza, I. Ahmad, B. Amin, A. Afaq, M. Maqbool, J. Maqssod, I. Khan, M. Zahid, Investigation of structural and optoelectronic properties of $BaThO_3$. Opt. Mater. **33**, 553–557 (2011)
22. J.G. Bednorz, K.A. Müller, Perovskite-type oxides—the new approach to high-T_c superconductivity. Rev. Mod. Phys. **60**, 585 (1988)
23. S. Jin, T.H. Tiefel, M. McCormack, R.A. Fastnacht, R. Ramesh, L.H. Chen, Thousandfold change in resistivity in magnetoresistive La–Ca–Mn–O films. Science **264**, 413–415 (1994)
24. M. Manzoor, S. Chowdhury, R. Sharma, M.W. Iqbal, S.K. Mukherjee, S.S. Alarfaji, H.A. Alzahrani, Insight on the lattice dynamics, thermodynamic and thermoelectric properties of $CdYF_3$ perovskite: a DFT study. Comput. Theor. Chem. **1217**, 113928 (2022)
25. S.A. Dar, V. Srivastava, U.K. Sakalle, A First-principles calculation on structural, electronic, magnetic, mechanical, and thermodynamic properties of $SrAmO_3$. J. Supercond. Novel Magn. **30**, 3055–3063 (2017)
26. A.H. Reshak, D. Stys, S. Auluck, I.V. Kityk, Dispersion of linear and nonlinear optical susceptibilities and the hyperpolarizability of 3-methyl-4-phenyl-5-(2-pyridyl)-1, 2, 4-triazole. Phys. Chem. Chem. Phys. **13**, 2945–2952 (2011)
27. A. Souidi, S. Bentata, W. Benstaali, B. Bouadjemi, A. Abbad, T. Lantri, First principle study of spintronic properties for double perovskites Ba_2XMoO_6 with X = V, Cr and Mn. Mater. Sci. Semicond. Process. **43**, 196–208 (2016)
28. P. Blaha, K. Schwarz, P. Sorantin, S.B. Trickey, Full-potential, linearized augmented plane wave programs for crystalline systems. Comput. Phys. Commun. **59**, 399–415 (1990)
29. P. Blaha, K. Schwarz, G.K.H. Madsen, D. Kvasnicka, J. Luitz, wien2k. An Augmented Plane Wave+ Local Orbitals Program for Calculating Crystal Properties. 60 (2001)
30. J.P. Perdew, K. Burke, M. Ernzerhof, Generalized gradient approximation made simple. Phys. Rev. Lett. **77**, 3865 (1996)
31. T. Charpin, *A Package for Calculating Elastic Tensors of Cubic Phase Using WIEN* (Laboratory of Geometrix, Paris, 2001)
32. F.D. Murnaghan, The compressibility of media under extreme pressures. Proc. Natl. Acad. Sci. **30**, 244–247 (1944)
33. M. Łopuszyński, J.A. Majewski, Ab initio calculations of third-order elastic constants and related properties for selected semiconductors. Phys. Rev. B **76**, 45202 (2007)
34. N. Bouarissa, S. Saib, Elastic modulus, optical phonon modes and polaron properties in $Al_{1-x}B_xN$ alloys. Curr. Appl. Phys. **13**, 493–499 (2013)
35. A.A. Maradudin, E.W. Montroll, G.H. Weiss, I.P. Ipatova, *Theory of Lattice Dynamics in the Harmonic Approximation* (Academic press, New York, 1963)
36. M. Flórez, J.M. Recio, E. Francisco, M.A. Blanco, A.M. Pendás, First-principles study of the rocksalt–cesium chloride relative phase stability in alkali halides. Phys. Rev. B **66**, 144112 (2002)
37. S. Zhao, Z. Wei, S.A. Dar, Insight into the structural, electronic, elastic, mechanical, and thermodynamic properties of $XReO_3$ (X = Rb, Cs, Tl) perovskite oxides: a DFT study. Z. Naturforschung A **74**, 827–836 (2019)
38. D. Behera, R. Sharma, H. Ullah, H.S. Waheed, S.K. Mukherjee, Electronic, optical, and thermoelectric investigations of Zintl phase AAg_2Se_2 (A = Sr, Ba) compounds: a first first-principles approach. J. Solid State Chem. **312**, 123259 (2022)
39. D. Behera, M. Manzoor, M.W. Iqbal, S. Lakra, S.K. Mukherjee, Revealing excellent electronic, optical, and thermoelectric behavior of Eu based EuAg2Y2 (Y= S/Se): For solar cell applications. Comput. Condensed Matter **32**, e00723 (2022)
40. M. Manzoor, D. Bahera, R. Sharma, F. Tufail, M.W. Iqbal, S.K. Mukerjee, Investigated the structural, optoelectronic, mechanical, and thermoelectric properties of Sr_2BTaO_6 (B = Sb, Bi) for solar cell applications. Int. J. Energy Res. (n.d.)
41. J.A. Abraham, D. Behera, K. Kumari, A. Srivastava, R. Sharma, S.K. Mukherjee, A comprehensive DFT analysis on structural, electronic, optical, thermoelectric, SLME properties of new Double Perovskite Oxide Pb_2ScBiO_6. Chem. Phys. Lett. **806**, 139987 (2022)
42. D. Behera, S.K. Mukherjee, Theoretical investigation of the lead-free K_2InBiX_6 (X = Cl, Br) double perovskite compounds using first principle calculation. JETP Lett. 1–10 (2022)
43. M. Born, On the stability of crystal lattices. I. in *Mathematical Proceedings of the Cambridge Philosophical Society* (Cambridge University Press, 1940), pp. 160–172
44. I. Waller, Dynamical theory of crystal lattices by M. Born and K. Huang. Acta Crystallogr. **9**, 837–838 (1956)
45. D. Behera, S.K. Mukherjee, Optoelectronics and transport phenomena in Rb_2InBiX_6 (X = Cl, Br) compounds for renewable energy applications: a DFT insight. Chemistry **4**, 1044–1059 (2022)
46. R. Hill, The elastic behaviour of a crystalline aggregate. in *Proceedings of the Physical Society*. Section A., vol. 65 (1952), p. 349
47. S.F. Pugh, XCII. Relations between the elastic moduli and the plastic properties of polycrystalline pure metals. Lond. Edinb. Dublin Philos. Mag. J. Sci. **45**, 823–843 (1954)
48. S.A. Dar, V. Srivastava, U.K. Sakalle, V. Parey, Electronic structure, magnetic, mechanical and thermo-physical behavior of double perovskite Ba_2MgOsO_6. Eur. Phys. J. Plus **133**, 1–12 (2018)
49. M.A. Blanco, E. Francisco, V. Luana, GIBBS: isothermal-isobaric thermodynamics of solids from energy curves using a quasi-harmonic Debye model. Comput. Phys. Commun. **158**, 57–72 (2004)
50. R. Vali, Lattice dynamics of cubic $SrZrO_3$. J. Phys. Chem. Solids **69**, 876–879 (2008)
51. S.A. Dar, V. Srivastava, U.K. Sakalle, Ab initio high pressure and temperature investigation on cubic $PbMoO_3$ perovskite. J. Electron. Mater. **46**, 6870–6877 (2017)
52. A. Otero-de-la-Roza, V. Luaña, Equations of state and thermodynamics of solids using empirical corrections in the quasiharmonic approximation. Phys. Rev. B **84**, 184103 (2011)

53. D. Bahera, A. Dixit, B. Nahak, A. Srivastava, S. Dubey, R. Sharma, A.K. Mishra, S.K. Mukeerjee, Structural, electronic, elastic, vibrational and thermodynamic properties of antiperovskites Mg_3NX (X = Ge, Sn): a DFT study. Phys. Lett. A **453**, 128478 (2022)
54. Z. Wan, Y. Yu, H.F. Zhang, T. Gao, X.J. Chen, C.J. Xiao, First-principles study of electronic, dynamical and thermodynamic properties of Li_2TiO_3. Eur. Phys. J. B **85**, 1–7 (2012)
55. P.L. Dulong, A.-T. Petit, Recherches sur quelques points importans de la theorie de la chaleur (1819)